Structural characterization and photochemical properties of mono-and bimetallic Cu-Mabiq complexes

H. Sophia Stark,[†] *Philipp Altmann,*[†] *Stephen Sproules,*[§] *and Corinna R. Hess**[*,†]

[†]Department of Chemistry and Catalysis Research Center, Technische Universität München, Lichtenbergstraße 4, D-85747 Garching, Germany

[§]WestCHEM, School of Chemistry, University of Glasgow, Glasgow, G12 8QQ, United Kingdom

Abstract. We present a series of monometallic ([Cu(Mabiq)OTf] (**1**) and [Cu(Mabiq)] (**2**)) and bimetallic copper-Mabiq complexes ($[Cu_2(Mabiq)(PPh_3)_2(OTf)_2]$ (**3**) and $[Cu_2(Mabiq)(PPh_3)_2]PF_6$ (**4**). The latter compounds contain an additional Cu^I center that binds in a tetrahedral fashion to the external bipyrimidine nitrogens of the macrocyclic ligand. Compounds **3** and **4** represent the first examples of bimetallic transition metal Mabiq complexes, stable both in solution and in the solid state. The structural and electronic properties of compounds **1** – **4** were analyzed by means of X-ray crystallography, cyclic voltammetry and spectroscopic methods. One-electron reduced **2** and **4** consist of a Cu^{II} ion coordinated by a Mabiq ligand radical, $[Cu^{II}(Mabiq^{\bullet})]$. Thus, both bimetallic compounds are mixed valent with respect to the copper oxidation states. The formally Cu^I complexes can also be generated photochemically, upon irradiation of **1** or **3** with visible light in the presence of a sacrificial electron donor.

Introduction. Tetraaza-macrocyclic metal centers feature prominently among enzymes, and therein support diverse functions that include O_2 activation (heme centers), isomerization reactions (vitamin B_{12}) and light harvesting (chlorophylls).[1-8] The chemistry and photochemical properties of these cofactors have inspired the synthesis of tetraazamacrocyclic metal complexes for over a century.[9-13] To date, the structural and functional diversity within this family of synthetic compounds is vast. The biomimetic porphyrins, corrins and phthalocyanins represent cornerstone molecules among a growing number of related, yet more complex, scaffolds.[14-21] The corresponding coordination complexes mimic many properties of their biological counterparts, including photosensitizer capabilities and reactivity toward small molecules.[21-25] However, the array of N_4-macrocyclic compounds also continue to yield new reactivities and wide-ranging applications in areas ranging from catalysis,[26-27] to solar cell and photodiode technologies,[28-29] to medical applications.[30-31]

Over the past years, we have examined the coordination chemistry and redox properties of a macrocyclic biquinazoline ligand, Mabiq.[32] This ligand resembles the more common corrins and phthalocyanines, and has several notable features. The molecule is redox-active, giving rise to characteristic electronic structures and offering an additional electron storage site in the reactivity of the corresponding metal compounds.[33-35] The molecule also exhibits promise for photoredoxcatalysis, as recently demonstrated for the $[Ni^{II}(Mabiq)]^+$ complex.[36] Furthermore, the Mabiq ligand is distinct from the majority of N_4-macrocycles in that it provides a second peripheral metal binding site. This latter feature has so far been underexplored. Our studies have primarily focused on the characterization of the monometallic compounds, although binding of cobalt and sodium ions to the second coordination site was observed in several cases.[34-35] The established properties of the Mabiq ligand and the availability of the second metal binding site opens new

avenues for reactivity, including the potential for bifunctional (photo)catalysis. Thus, we recently turned our attention to the synthesis and study of bimetallic Mabiq complexes. We herein present a series of mono- and bimetallic Cu-Mabiq compounds, which include mixed valent $Cu^{I}Cu^{II}$ forms. The synthesis and redox properties of the complexes are described, along with results of preliminary studies examining their photochemical properties.

Synthesis and Solid-State Structures. The monometallic copper complexes were synthesized in straightforward reactions of the macrocyclic ligand with various copper salts (Scheme 1). The reaction of HMabiq with $Cu(OTf)_2$ yielded the brown solid [Cu(Mabiq)OTf] (**1**), whereas the one-electron reduced [Cu(Mabiq)] (**2**) was synthesized using $[Cu(MeCN)_4]PF_6$ as the Cu^{I} source. Compound **2** alternatively can be generated upon reduction of **1** with one equiv. of Na/Hg. The copper-containing compounds complete the M^{II} and formally M^{I} series of late first-row transition metal Mabiq complexes. The sequence of complexes permits an evaluation of periodic trends in redox properties, electronic structures and reactivity among M-Mabiq complexes.

The presence of the external bipyrimidine binding site of the Mabiq ligand inspired a strategy to incorporate a copper-based photosensitizer at this position and, thereby, generate potential binuclear photocatalysts. A binuclear Co-Mabiq complex, $[Co_2(Mabiq)Cl_3]$, was previously isolated, but appeared to suffer from solution instability. However, heteroleptic Cu^{I} photosensitizers based on phenanthroline and phosphine ligands are well-known.[37-45] We speculated that a cuprous ion could be stably supported with a comparable coordination environment – supplied by the Mabiq bipyrimidine group and added triphenylphosphines – and that this second copper unit might exhibit similar luminescence properties. The reaction of **1** with $[Cu(MeCN)_4]OTf$ and two equivalents of PPh_3 yielded the binuclear $[Cu_2(Mabiq)(PPh_3)_2(OTf)_2]$

(**3**), isolated as an orange solid. The one-electron reduced, green solid $[Cu_2(Mabiq)(PPh_3)_2]PF_6$ (**4**) can be generated upon reaction of HMabiq with two equivalents of $[Cu(MeCN)_4]PF_6$ and PPh_3. Improved yields of **4** were obtained by addition of $Cu(PPh_3)_3PF_6$ to **2**. The solid-state composition of the dicopper complexes was verified by elemental analysis, alongside other analytical methods as described below.

Molecular structures were obtained for all compounds **1** – **4** (Figure 1, Tables S1–S3). The copper bound within the macrocyclic cavity of **1** (Cu_c) adopts a square pyramidal coordination geometry, with a weakly bound triflate ion in the axial position (Cu_c–O1A = 2.497(4) Å), whereas compound **2** is square planar. The Cu_c–N bond distances are comparable in the two complexes (**1**: Cu_c–$N_{(bpm)avg}$ = 1.955 Å, Cu_c–$N_{(diketim)avg}$ = 1.920 Å; **2**: Cu_c–$N_{(bpm)avg}$ = 1.952 Å, Cu_c–$N_{(diketim)avg}$ = 1.921 Å).[46] In contrast, considerable differences in the C–N bond distances of the diketiminate unit and bridging imines of **1** and **2** are observed (Table S1). The data suggest that both compounds contain a cupric ion, such that **2** may be described as $[Cu^{II}(Mabiq^{\bullet})]$ instead of $[Cu^{I}(Mabiq)]$.[47] The former formulation is consistent with our previous findings that the formally M^{I}-Mabiq complexes, across the series M = Fe, Co, Ni, Zn, possess substantial ligand radical character.[33-34] In addition to the altered Mabiq bond distances, reduction of the ligand coincides with significant buckling of the macrocycle: a ~16° coplanarity difference between the two quinazoline groups of **2** is observed, vs. ~2° in complex **1**.

The outer metal center (Cu_o) assumes a tetrahedral geometry in the bimetallic complexes **3** and **4**. Binding of the second copper ion has only a minor effect on the coordination environment of the central copper site. The geometry of Cu_c in **4** is identical to that of the metal center in **2**, whereas the cupric ion of **3** coordinates an additional triflate ion (Cu_c–O_{avg} = 2.562 Å). The Cu_c–N distances of **3** and **4** are similar to each other, and to their monometallic counterparts (**3**: Cu_c–$N_{(bpm)avg}$ =

1.955 Å, Cu_c–$N_{(diketim)avg}$ = 1.904 Å; **4**: Cu_c–$N_{(bpm)avg}$ = 1.954 Å, Cu_c–$N_{(diketim)avg}$ = 1.920 Å). The Cu···Cu distances are 5.4602(8) Å and 5.4160(6) Å in **3** and **4**, respectively.

Solution state characterization. Each of the four copper complexes exhibit unique electronic spectra (Figure 2), but also share several spectral features with previously isolated M-Mabiq compounds.[32-35] The intense π–π* transitions seen in the UV-visible region for **1** and **2** are common among the spectra of M-Mabiq complexes. The visible-NIR bands of **2** (600 – 2200 nm; Figure S1) typify neutral [M^{II}(Mabiq$^{\bullet}$)] species, such that across the M-Mabiq series, ligand-centered reduction is favoured over metal-centered reduction, even for the copper compounds. The absorption spectra of the binuclear **3** and **4** differ markedly from those of **1** and **2**, as well as of [$Cu(PPh)_3$]PF_6, an indication that both metal ions remain associated with the ligand in solution. The bands in the UV-visible region exhibit greater complexity and a decreased intensity vs. their monometallic counterparts. These absorptions may encompass Cu^{I}_{o} → bpm MLCT transitions in addition to ligand-centered transitions, as [$(phen)Cu(PPh_3)_2$]$^+$ compounds possess MLCT bands in this region.[37-38, 40, 48] Compound **4** also exhibits the visible-NIR bands indicative of Mabiq-centered reduction (Figure 2, Figures S1 and S2), but their absorbance, likewise, is significantly diminished in comparison to the spectrum of **2**.

Cyclic voltammetry (CV) data for compounds **1** – **4** (Figure 3; Table 1) provide further information on the redox properties of the complexes, as well as insight into the influence of Cu_o on the redox behaviour of Cu_c. The CV of **1** displays two reversible reductions at −1.22 V and −2.15 V vs. $Fc^{+/0}$ (THF), along with an additional irreversible reductive event below −2.5 V (Figure S3). An oxidative event, corresponding to the $Cu^{III/II}$ couple, can be observed at 1.32 V for CVs in MeCN (Figure S4). Three redox couples appear in the CV of the four-coordinate square planar **2**

but are shifted to significantly more positive potentials vs. the corresponding couples of the five-coordinate **1**. The redox events at −1.22 and −0.49 V in the CVs of **1** and **2**, respectively, are each associated with the formal $Cu^{II/I}$ couple but, more likely (vide supra), involve ligand-centered processes corresponding to the Mabiq/Mabiq$^{\bullet}$ couple. The last reductions likely then yield a $[Cu^{I}(Mabiq^{\bullet\bullet})]^{2-}$ species; evidence for a Mabiq-biradical was observed in our studies with the Co-Mabiq compounds.[34]

The effect of coordination of Cu_o is evident in the electrochemical data for **3** and **4**: the redox couples are generally shifted to more positive potentials vs. those of the monometallic counterparts (Table 1), but all remain reversible. The dicopper complexes exhibit irreversible oxidative processes in the region from 0.5 – 1.5 V that correspond to the $Cu_o^{II/I}$ and $Cu_c^{III/II}$ couples (Figure S4, MeCN). However, these processes cannot be differentiated, as the oxidation of Cu^{I}-phenanthroline compounds similarly occurs at potentials greater than 0.5 V vs. $Fc^{+/0}$.[40, 49-50] Overall, a wide range of oxidation states is available for the series of mono- and bimetallic copper compounds, which may offer advantages for reactivity.

As expected, complexes **1** and **3** are paramagnetic with an $S = {}^{1}/_{2}$ ground state. The EPR spectrum of **1** recorded in dichloromethane solution at room temperature bears the hallmark four-line pattern resulting from the hyperfine coupling of the Cu^{II} electron spin with the $I = {}^{3}/_{2}$ nuclear spin of the $^{63,65}Cu$ isotopes (100% abundant). There is additional splitting on the lines to high field from superhyperfine coupling of all four nitrogen (^{14}N, $I = 1$, 99.7% abundant) donor atoms of the Mabiq ligand. Such a profile is very familiar in macrocyclic CuN_4 complexes.[51-52] The spectrum was simulated yielding spin-Hamiltonian parameters: $g_{iso} = 2.0782$; $A_{Cu} = 87 \times 10^{-4}$ cm^{-1}; $A_N = 14.5 \times 10^{-4}$ cm^{-1} (Figure 4). The addition of THF to this sample of **1** afforded a homogeneous frozen glass at 140 K. The spectrum is quintessentially that of a Cu^{II} species with an unpaired electron in the

$d_{x^2-y^2}$ orbital ($^2B_2$ ground state) with anisotropic spin-Hamiltonian parameters for Cu: g = (2.037, 2.040, 2.153); A_{Cu} = (25, 22, 218) × 10^{-4} cm^{-1}. The glassing solvent mixture ensured resolution of the superhyperfine interaction with the N-donor atoms of Mabiq which is seen as an 11-line splitting of each of the $A_{||}$ lines and the central $g_{\perp}$ feature with magnitude, A_N = (13, 13, 12) × 10^{-4} cm^{-1}. The EPR spectrum of **3** is not surprisingly similar to that of **1** giving nearly identical spin-Hamiltonian parameters for both fluid solution (g_{iso} = 2.0788; A_{Cu} = 83 × 10^{-4} cm^{-1}; A_N = 14.8 × 10^{-4} cm^{-1}) and frozen glass spectra (g = (2.037, 2.040, 2.160); A_{Cu} = (20, 17 214) × 10^{-4} cm^{-1}; A_N = (13, 13, 12) × 10^{-4} cm^{-1}; Figure 4). The salient difference at room temperature are the broader lines and consequently less resolved ^{14}N superhyperfine splitting. This stems from the inclusion of a $\{Cu^I(PPh_3)_2\}$ moiety which perturbs the motional tumbling of this molecule in solution as this is the mechanism that governs linewidth. In frozen solution, it is the uniformity of the glass which does lead to a slight line broadening in the spectrum of **3** though the ^{14}N superhyperfine splitting remains visible for all features across the spectrum.

Solutions of the one-electron reduced forms **2** and **4** neither exhibit EPR signals nor any discernible ^1H NMR resonances. The room temperature magnetic moment values, as determined by the Evans method, are 1.8 ± 0.08 μ_B and 2.0 ± 0.03 μ_B,[53] respectively. As previously noted, the structural and spectroscopic data imply that both complexes are comprised of the reduced Mabiq ligand ligated to a Cu^{II}_c ion. DFT (B3LYP) calculations were carried out on **1** – **4** to further probe their electronic structures (Figures S5 – S7, Tables S4 – S9). Both the S_T = 0 and S_T = 1 ground states of **2** were examined. For the S_T = 0 configuration, the BS(1,1) approach provided a lower energy solution vs. the UKS calculation, which nevertheless yielded an open-shell solution and an identical electronic structure. The triplet (UKS) and open-shell singlet BS(1,1) species are near-degenerate (ΔE (S_T = 1 – S_T = 0) = 0.5 kcal mol^{-1}). In each case, one metal-centered and one ligand-

centered SOMO can be identified (Figure 5), with a spatial overlap of S = 0.29. The ligand-centered SOMO is largely distributed over the diketiminate unit, but also encompasses π-based orbitals of the opposing bipyrimidine. The unpaired electron on the Cu^{II} center resides in the d_{x2-y2} orbital, as was determined for **1** (vide supra). Analogous calculations were carried out on the bimetallic **4** and yielded similar results (Figures S6 and S7). The calculated $S = 0$ and $S = 1$ ground state are likewise degenerate (0.7 kcal mol^{-1}), and the electronic structures are consistent with the $[Cu_o(\uparrow\downarrow)(Cu_c\uparrow)(Mabiq\downarrow)]^+$ or $[Cu_o(\uparrow\downarrow)(Cu_c\uparrow)(Mabiq\uparrow)]^+$ formulations of **2**. The presence of the external Cu^I_o ion has no impact on the nature of the SOMOs. Although we currently cannot unambiguously explain the magnetic moments obtained for **2** and **4**, which lie in between the expected values for an $S = 0$ and $S = 1$ state, contributions from the triplet and singlet forms of the compounds may account for the unusual magnetic moment values.

Photochemical properties. The photochemical properties of Cu-phenanthrolines are well-established, while Cu^I-phthalocyanins show only very weak fluorescence.[54] We thus examined the steady state luminescence of **1** — **4**, as well as of the metal-free HMabiq molecule, to assess the capacity of our compounds to act as photosensitizers. HMabiq exhibits an emission band at 521 nm, corresponding to the excitation at 506 nm (Figure 6 and Figure S8). The 506 nm band in the absorption spectrum of HMabiq appears as a shoulder to the broad, more intense transitions that span the UV-visible region. Compound **1** also fluoresces at a similar wavelength, but the fluorescence is substantially reduced compared to that of the free ligand. Complexes **2** — **4** do not exhibit any appreciable steady state emission. One might expect that any luminescence exhibited by the HMabiq ligand would be retained upon coordination of a genuine Cu^I d^{10} ion. The absence of any observable luminescence by **2** and **4** further supports the Cu^{II}-(Mabiq$^\bullet$) character of the

complexes. Emission due to the Cu^{I}_{o} site also was not observed. The heteroleptic Cu-phosphine-phenanthroline photosensitizers, as well as pyrimidine-based analogues, typically display broad emission bands at 600 nm, originating from MLCT transitions centered at ca. 450 nm in their absorption spectra.[37, 44, 55] The absence of any steady-state emission for **3** and **4** suggests effective quenching of the Cu_o fluorescence by the Cu_c.

Previous studies have shown that it is possible to photoreduce the Ni^{II}-Mabiq complex upon irradiation with visible light in the presence of a sacrificial electron donor.[36] We thus examined whether the cupric containing **1** and **3** exhibited similar photochemical behaviour (Scheme 2). Indeed, both complexes **1** and **3** can be reduced to **2** and **4** upon irradiation (λ = 457 nm; LED see SI for details) in the presence of triethylamine (NEt_3) as the sacrificial reductant. The photoreduction of **1**, monitored by absorption spectroscopy, was complete within 20 min, while only 59% conversion of **3** to **4** was achieved in the same time period (Figure 7 and Figure S9; λ = 457 nm, [**1**, **3**] = 0.13 mM; [NEt_3] = 0.5 M in DMF). The photoreduction of **1** also could be followed by EPR spectroscopy, which shows the disappearance of the Cu^{II}-Mabiq signal over several minutes ([**1**] = 0.6 mM; [NEt_3] = 0.72 M in MeCN); Figure S10). Quantum yields of the photoreduction were determined for both **1** and **3** ([**1**, **3**] = 0.67 mM; [NEt_3] = 2.3 M in DMF; λ = 457 nm). A higher quantum yield is obtained for the photoreduction of **1** ($\Phi = 1.2 \times 10^{-3} \pm 9 \times 10^{-5}$; Figure S12) versus the bimetallic **3** ($\Phi = 5.4 \times 10^{-5} \pm 9 \times 10^{-6}$; Figure S13). The two copper centers clearly influence each other, as evidenced by the differing quantum yields of the mono- vs bimetallic complexes. Importantly, however, the presence of the outer copper center does not preclude photoreduction of the central metal ion. At a slightly shorter wavelength (λ = 415 nm) the quantum yields also are nearly identical for the mono- and bimetallic complexes ($\Phi = 6.0 \times$

10^{-4} and $\Phi = 1.6 \times 10^{-4}$ for **1** and **3**, respectively). An examination of the nature and lifetimes of the excited states of the Cu and related Mabiq compounds is currently underway.

Conclusions.

The Cu-Mabiq complexes presented herein complete the series of late transition metal complexes of this unique ligand scaffold. The compounds share a number of features with other M-Mabiq complexes, including preferential reduction of the Mabiq diketiminate moiety over metal-centered reduction. The dicopper complexes **3** and **4** provide the first examples of stable transition metal bimetallic Mabiq compounds, and have therefore enabled us to examine the influence of the second metal center on the properties of the central metal ion; a key facet for the further development of these systems as bifunctional catalysts. The addition of Cu^{I}_{o} has only a minor effect on the redox potentials of Cu_c and does not alter the electronic structure of the reduced $Cu^{II}(Mabiq^{\bullet})$ unit. The bipyrimidine group of the Mabiq ligand, thus, does not appear to mediate strong coupling between the two metal ions. The photochemical properties exhibited by the Cu-Mabiq unit also are retained, with only a moderate effect of Cu_o on the quantum yields for the photoreduction process. The data suggest that each individual metal ion can be further tuned for distinct functions without adversely affecting the neighboring site. As such, one can envision several roles for the individual metal centers in promoting reactivity. For example, through the judicious choice of conditions, M_c could act as a photosensitizer in conjunction with M_o as a catalytically active site, taking advantage of the less constrained coordination environment of the outer binding site. Alternatively, M_o could be used to incorporate pendant groups, position substrates or introduce steric constraints in order to enhance reactivity occurring at the M_c. With a

greater understanding of the bimetallic Mabiq systems, we now turn our attention to exploring these aspects.

EXPERIMENTAL

General Procedures. $Cu(OTf)_2$, Cu(OTf), triphenylphosphine and triethylamine were purchased from Sigma Aldrich, and $[Cu(MeCN)_4]PF_6$ was purchased from Strem Chemicals. Solvents were dried by passage over activated alumina columns, deoxygenated and stored over activated 3 or 4 Å molecular sieves prior to use. All metal complexes were synthesized under an inert atmosphere. $[Cu(PPh_3)(MeCN)]PF_6$ was synthesized according to literature procedure.[56] H(Mabiq) was synthesized as previously described.[32, 34] Tetrabutylammonium hexafluorophosphate was recrystallized three times from ethanol and Ferrocene was sublimated prior to use.

Cu(Mabiq)OTf (**1**). Triethylamine (12 μL, 0.13 mmol) was added to a solution of H(Mabiq) (70.0 mg, 0.13 mmol) in dichloromethane (10 mL), and $Cu(OTf)_2$ (46.3 mg, 0.13 mmol) was added subsequently. The solution quickly turned dark red and, after stirring for 18 hours, was dark brown. The product solution was filtered over Celite. Single crystals suitable for X-ray diffraction and used for all other data analysis (98.9 mg, 0.11 mmol, 89% yield) were obtained by slow diffusion of pentane into the crude product solution. When used for measurements other than X-ray diffraction, the crystals were washed with pentane and diethyl ether and dried under vacuo. The unit cell contains one molecule of dichloromethane per molecule of **1**. Anal. Calcd for $C_{35}H_{35}Cl_2CuF_3N_8O_3S$ (**1**·CH_2Cl_2): C, 50.09; H, 4.20; N, 13.35. Found: C, 50.09; H, 4.21; N, 13.32. ESI-MS(+): m/z 604 ($[M]^+$). UV-Vis [λ_{max}, nm (ε, M^{-1} cm^{-1}), THF]: 268 (5.9 x 10^4), 340 (3.3 x 10^4), 471 (2.2 x 10^4).

Cu(Mabiq) (**2**). Triethylamine (21 μL, 0.14 mmol) was added to a solution of H(Mabiq) (75 mg, 0.14 mmol) and acetonitrile (10 mL), and $Cu(MeCN)_4PF_6$ (52 mg, 0.14 mmol) were added subsequently. The solution was stirred overnight, resulting in a green suspension. The precipitate

was filtered off and washed with acetonitrile, yielding a green powder (yield = 62%). Single crystals suitable for X-ray diffraction were obtained by the addition of pentane into a solution of **2** in THF. Alternatively, Na/Hg (5%, 38 mg, 0.09 mmol) was added to a solution of **1** (50 mg, 0.09 mmol) in 10 mL MeCN. After 18 hours of vigorous stirring, the green precipitate was filtered over a sintered glass filter and washed with 20 mL MeCN. A higher purity sample could be obtained when the green powder was dissolved in THF and filtered over Celite. Anal. Calcd for $C_{33}H_{33}CuN_8$ (**2**): C, 65.49; H, 5.50; N, 18.51. Found: C, 65.21; H, 5.75; N, 18.38. ESI-MS (+): m/z 604 ($[M]^+$). UV-Vis [λ_{max}, nm (ε, M^{-1} cm^{-1}), THF]: 258 (6.8 x 10^4), 336 (3.9 x 10^4), 353 (4.1 x 10^4), 416 (1.3 x 10^4), 683 (6.3 x 10^3), 752 (5.4 x 10^3), 1326 (2.7 x 10^3).

$Cu_2(Mabiq)(PPh_3)_2(OTf)_2$ (**3**). $Cu(MeCN)_4OTf$ (26 mg, 0.068 mmol) and PPh_3 (36 mg, 0.14 mmol) were added to a solution of **2** (57 mg, 0.07 mmol) in THF (10 mL). The brown solution turned dark red after 18 hours of stirring. The product solution was filtered over Celite. Single crystals suitable for X-ray diffraction were obtained by slow diffusion of pentane into a THF solution of **3**. When used for measurements other than X-ray diffraction, the crystals were washed with pentane and dried under vacuo (70 mg, 0.05 mmol, 74%). Anal. Calcd for $C_{72}H_{66}Cu_2F_6N_8O_6P_2S_2$: C, 57.18; H, 4.26; N, 7.51. Found: C, 57.00; H, 4.25; N, 7.62. (UV-Vis [λ_{max}, nm (ε, M^{-1} cm^{-1}), THF]: 273 (4.9 x 10^4), 362 (12.4 x 10^4), 469 (1.8 x 10^4).

$[Cu_2Mabiq(PPh_3)_2](PF_6)$ (**4**). $[Cu(PPh_3)_3(MeCN)]PF_6$ (67 mg, 0.07 mmol) was added to a solution of **2** (41 mg, 0.07 mmol) in THF (10 mL). After 18 hours of vigorous stirring, the light green solution became a dark green reaction mixture, which was filtered over Celite. Single crystals suitable for X-ray diffraction and all other data analysis were obtained by slow diffusion of pentane into the filtrate. When used for measurements other than X-ray diffraction, the crystals were washed with pentane and dried under vacuo (73.4 mg, 0.055 mmol, 82 % yield). The unit

cell contains one molecule of tetrahydrofuran per molecule of **4**. Anal. Calcd for $C_{73}H_{70}Cu_2F_6N_8OP_3$ (**4**·THF): C, 62.17; H, 5.07; N, 7.94. Found: C, 62.57; H, 5.25; N, 8.17. UV-Vis [λ_{max}, nm (ε, M^{-1} cm^{-1}), THF]: 257 (3.7 x 10^4), 355 (1.5 x 10^4), 386 (1.4 x 10^4), 686 (2.6 x 10^3), 759 (2.7 x 10^3), 888 (6.5 x 10^2), 1014 (6.2 x 10^2), 1202 (5.3 x 10^2), 1665 (5.7 x 10^2).

Physical measurements. X-band EPR spectra were recorded on a Bruker ELEXSYS E500 spectrometer, and simulations performed with Bruker's Xsophe software package.[57] X-band EPR spectra monitoring photoconversion were recorded on a Mini Scope MS5000EPR spectrometer in a sealed capillary. Solution state NMR spectra were recorded on a Bruker Avance Ultrashield (400 MHz ^{1}H). For determining magnetic susceptibility by the Evans method, cyclohexane was used as a reference. Electronic spectra were measured on a Shimadzu UV-3600 Plus UV-Vis-NIR spectrophotometer or an Agilent Cary 60 UV-Vis spectrophotometer. All absorption measurements were recorded after the acquisition of a baseline with pure solvent, or with the double beam setup with a solvent filled cuvette as the reference. UV Quartz cuvettes (190 – 2500 nm) with a 1 cm pathlength were used in all measurements. Luminescence spectra were recorded on a Varian Cary Eclipse Fluorescence Spectrophotometer under anaerobic conditions in THF (c(compound) = 0.05 mM). ESI mass spectra were measured on a Thermo Scientific™ UltiMate™ 3000 HPLYHPLC System using the loop mode. Microanalyses were carried out at the Technische Universität München. Electrochemical measurements were carried out with an EmStat^{3+} potentiostat using a three-electrode cell equipped with a glassy carbon working electrode and counter electrode and a Pt wire as reference electrode. Potentials are reported with reference to an internal standard of ferrocenium/ferrocene ($Fc^{+/0}$).

Crystallography. Crystallographic data were collected on an X-ray single crystal diffractometer equipped with a CMOS detector (Apex III, κ-CMOS), an IMS microsource with MoK_α radiation

(λ = 0.71073 Å) and a Helios mirror optic using the Apex III software package.[13, 58] The measurements were performed on a single crystal coated with perfluorinated ether. The crystal was fixed on top of a microsampler and transferred to the diffractometer. The crystal was frozen under a stream of cold nitrogen. A matrix scan was used to determine the initial lattice parameters. Reflections were merged and corrected for Lorenz and polarization effects, scan speed, and background using SAINT.[59] Absorption corrections, including odd and even ordered spherical harmonics were performed using SADABS.[59] Space group assignments were based upon systematic absences, E statistics, and successful refinement of the structures. Structures were solved by direct methods with the aid of successive difference Fourier maps, and were refined against all data using SHELXLE[60] in conjunction with SHELXL-2014.[61] Hydrogen atoms were assigned to ideal positions and refined using a riding model with an isotropic thermal parameter 1.2 times that of the attached carbon atom (1.5 times for methyl hydrogen atoms). If not mentioned otherwise, non-hydrogen atoms were refined with anisotropic displacement parameters. Full-matrix least-squares refinements were carried out by minimizing $\Sigma w(F_o^2-F_c^2)^2$ with SHELXL-97[62] weighting scheme. Neutral atom scattering factors for all atoms and anomalous dispersion corrections for the non-hydrogen atoms were taken from International Tables for Crystallography.[59]

Images of the crystal structures were generated by PLATON and Mercury.[63-64]

Density Functional Theory (DFT) Calculations. All DFT calculations were performed with the version 3.0.2 ORCA program package.[65-66] The input geometry for all molecules were defined by the crystallographic coordinated, and calculations utilized by the B3LYP[67-70] hybrid functional without imposing molecular symmetry. The all-electron Gaussian basis sets were those developed by the Ahlrich's group.[71-72] Triple-ζ quality basis sets (TZV(P)) with one set of polarization

functions[72] on the metals and on the atoms directly coordinated to the metal center were used for transition metal ions and all atoms other than carbon and hydrogen, for which the double-ζ basis sets with one set of polarization functions[71] (SVP) were used. The resolution of the identity approximation (RIJONX) was employed[73-77] with matching auxiliary basis sets.[76-77] SCF calculations were tightly converged (1×10^{-8} E_h in energy, 1×10^{-7} E_h in the density change, and 1×10^{-7} E_h in maximum element of the DIIS error vector). Geometry optimizations were carried out in redundant internal coordinates without imposing symmetry constraints. In all cases the geometries were considered converged after the energy change was less than 5×10^{-4} and 3×10^{-4} E_h $Bohr^{-1}$, respectively, and the root-mean square and maximum displacements of all the atoms were smaller than 2×10^{-3} and 4×10^{-3} Bohr, respectively. For calculations where the broken symmetry (BS) approach was used,[78-79] the notation BS(*m*,*n*) refers to a broken symmetry state with *m* unpaired α-spin electrons essentially on fragment 1 and *n* unpaired β-spin electrons localized on fragment 2. BS solutions were analyzed via the corresponding orbital transformation.[80-82] Orbital/spin density plots were created using VMD.[83]

ASSOCIATED CONTENT

Supporting Information. Crystallographic data files (CIF format) and additional electrochemical and spectroscopic data as well as DFT optimized coordinates.

CCDC 1824272-1824275 contain the supplementary crystallographic data for this paper. These data can be obtained free of charge via www.ccdc.cam.ac.uk/data_request/cif, or by emailing data_request@ccdc.cam.ac.uk, or by contacting The Cambridge Crystallographic Data Centre, 12 Union Road, Cam- bridge CB21EZ, UK; fax: + 44 1223 336033.

AUTHOR INFORMATION

Corresponding Author. E-mail: corinna.hess@ch.tum.de

ORCID.

Dr. Stephen Sproules: 0000-0003-3587-0375

Prof. Dr. Corinna R. Hess: 0000-0002-9607-9184

Notes. The authors declare no competing financial interest.

ACKNOWLEDGEMENT

HSS thanks the DBU (Deutsche Bundesstiftung Umwelt) and the TUM Graduate School for financial support. We are grateful to Dr. Alexander Pöthig and his team for Xray crystallography support, as well as to Dr. Andreas Bauer for technical support with the quantum yield

measurements. We thank Prof. Dr. Ueli Heiz for the use of the fluorimeter and Dr. Friedrich Esch for technical assistance with the benchtop EPR.

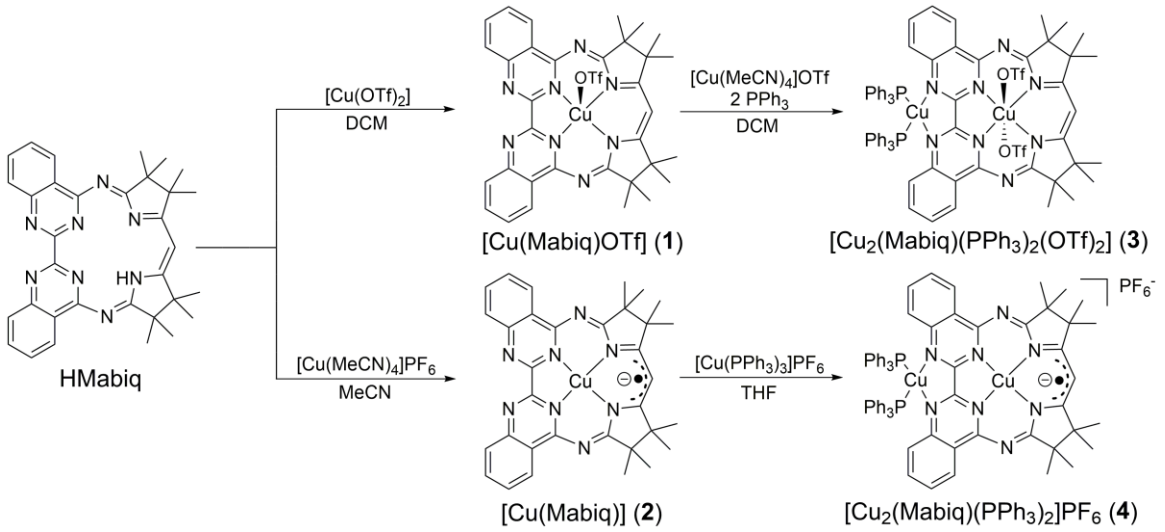

Scheme 1. Synthesis of mono- and bimetallic Cu-Mabiq compounds **1** – **4.**

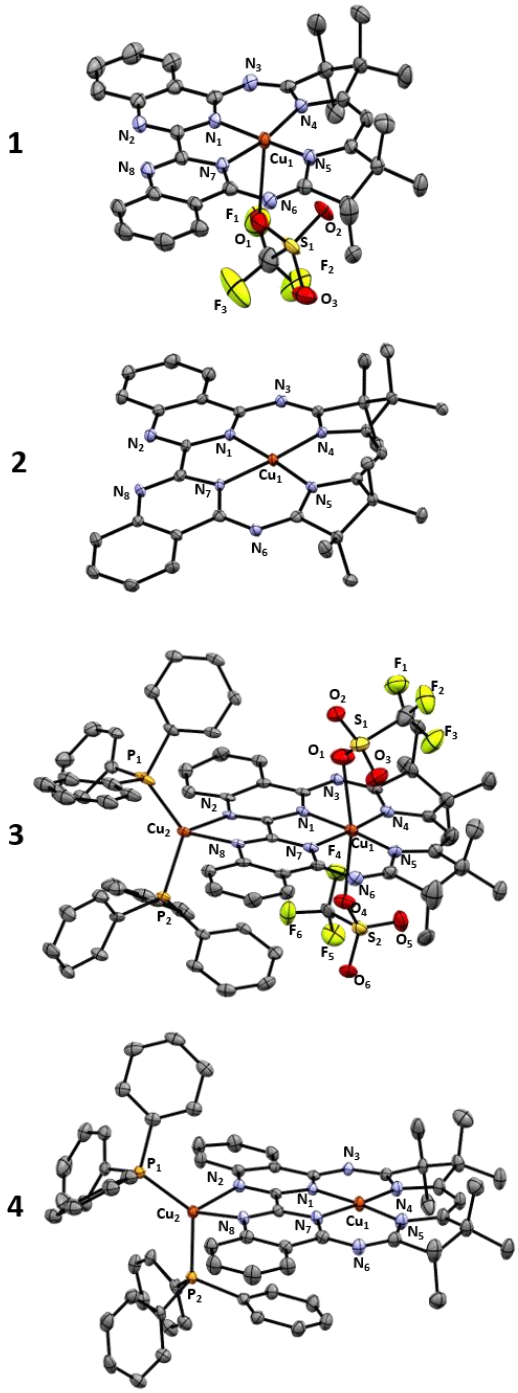

Figure 1. Molecular structures of **1** – **4** (50% probability ellipsoids). Hydrogen atoms, solvent molecules and non-coordinating counter ions are omitted for clarity.

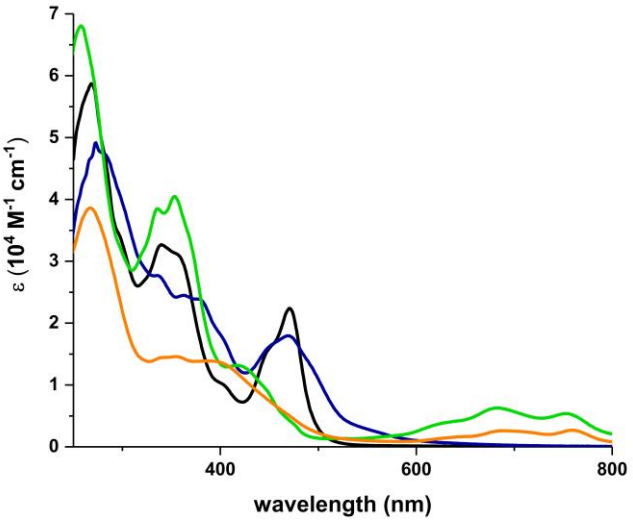

Figure 2. Electronic spectra of **1** (black), **2** (green), **3** (blue) and **4** (orange) in THF.

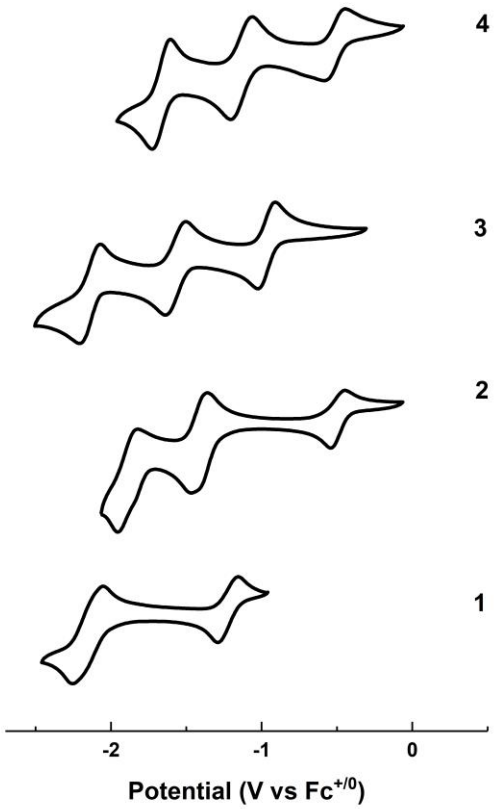

Figure 3. Cyclic voltammograms of **1** – **4** (0.1 V s^{-1}; 0.1 M $[N(n\text{-}Bu)_4]PF_6$; 0.5 mM of **1** – **4** in THF).

Table 1. Reduction Potentials (V vs Fc/Fc^{+}) of **1** – **4** in THF.

	$E_{1/2}$ (I)	$E_{1/2}$ (II)	$E_{1/2}$ (III)
1	-1.22	-2.15	
2	-0.49	-1.41	-1.89
3	-0.97	-1.57	-2.14
4	-0.54	-1.13	-1.67

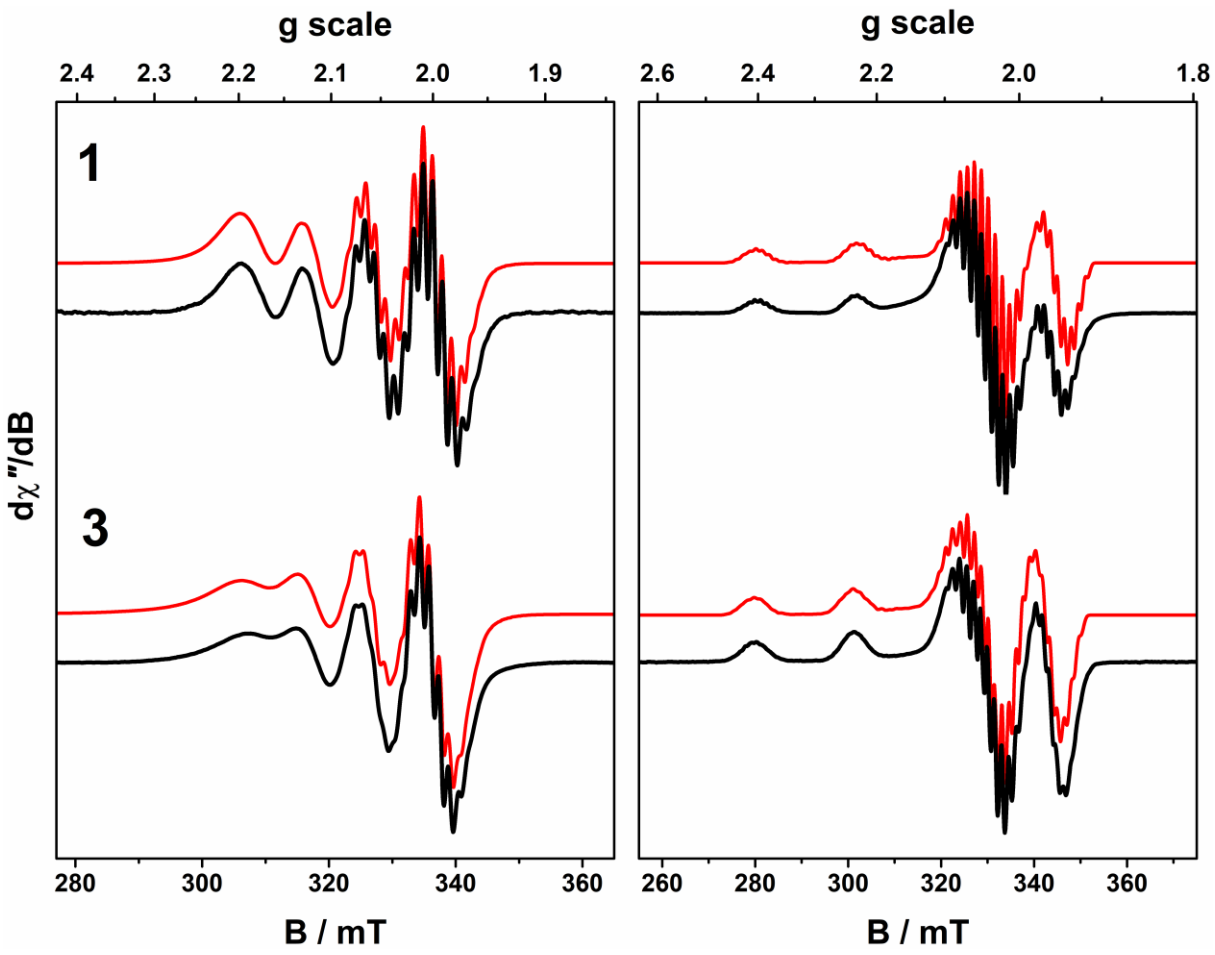

Figure 4. X-band EPR spectra of **1** and **3**. Left panel: CH_2Cl_2 solution at 293 K; right panel: CH_2Cl_2/THF frozen glass at 140 K. Experimental data are shown by the solid line; simulation depicted by the red trace (experimental conditions: frequency, 9.420 GHz; modulation, 0.2 mT; power, 0.63 mW).

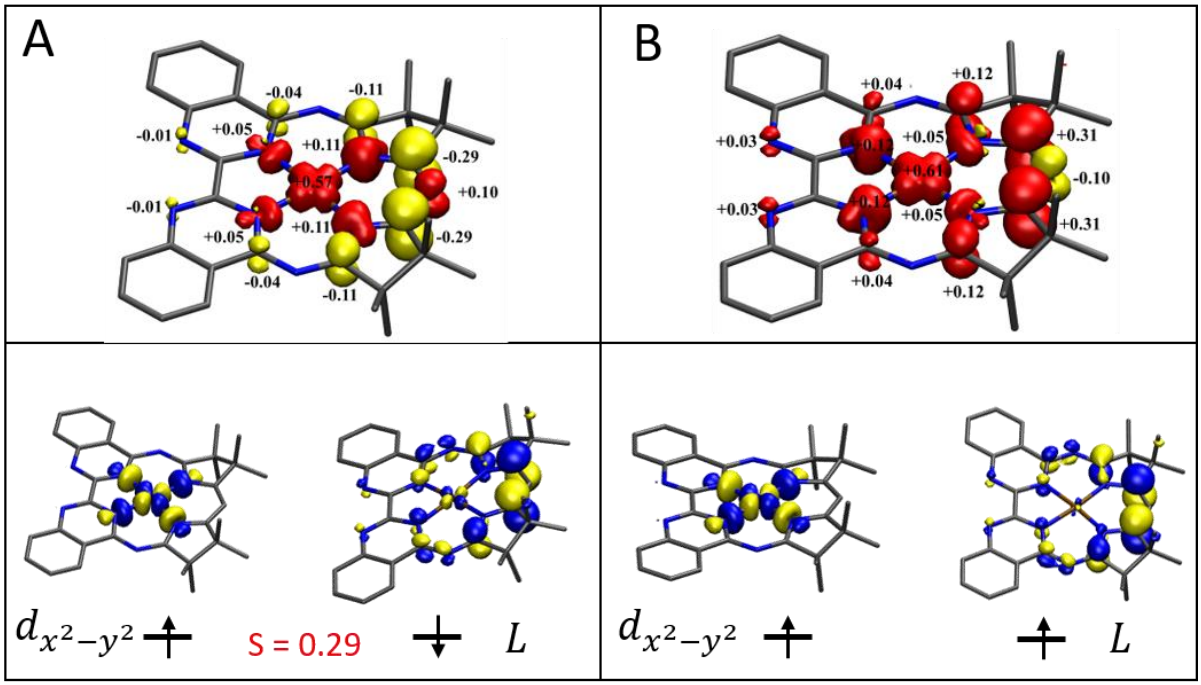

Figure 5. Top: DFT-derived (B3LYP) spin density plots for **2** based on Löwdin population analysis for A: S = 0 (BS(1,1) calculation); B: S =1 (UKS calculation). Bottom: DFT-derived (B3LYP) depiction of the SOMOs of **2**. A: S = 0 state, BS(1,1) with spatial overlap S; B: S = 1 state (UKS).

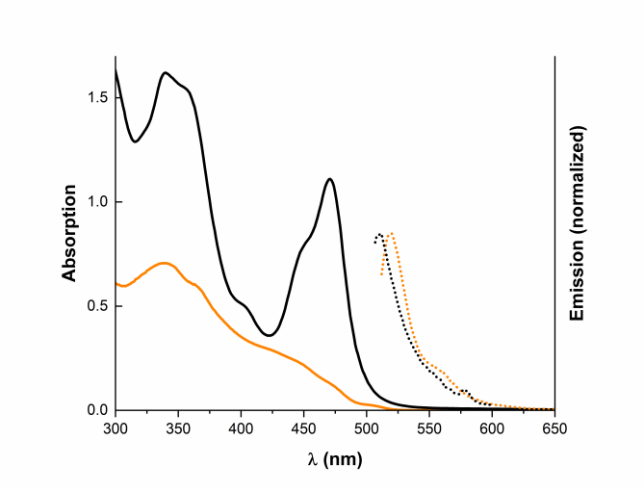

Figure 6. Absorption (—) and emission (···) spectra of HMabiq (orange, λ_{exc} = 506 nm, λ_{em} = 521 nm) and **1** (black, λ_{exc} = 497 nm, λ_{em} = 513 nm); c(**1**, HMabiq) = 0.05 mM in THF; room temperature; data acquired under anaerobic conditions. The respective fluorescence quantum yields are provided in the SI.

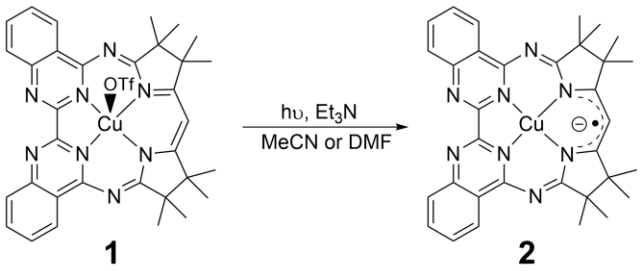

1 **2**

Scheme 2. Photoreduction of **1** to **2**. The same scheme applies for the reduction of **3** to **4**.

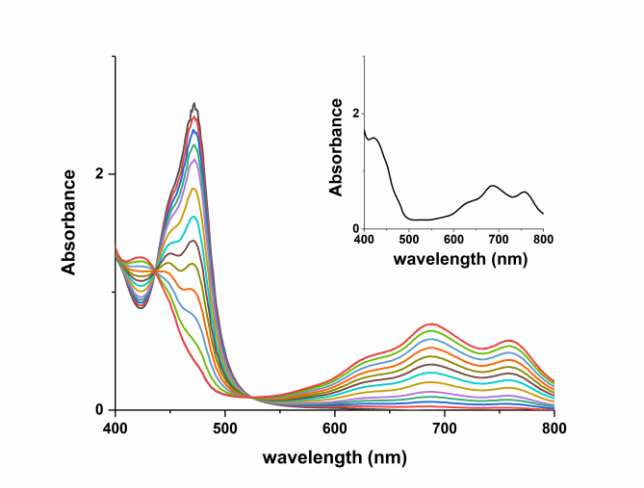

Figure 7. Spectral evolution during photoreduction of **1** over a period of 20 minutes ([**1**] = 0.13 mM; [NEt_3] = 0.5 M; DMF; λ = 457 nm). Inset depicts the spectrum of **2** ([**2**] = 0.13 mM; DMF) for reference.

REFERENCES.

1. Poulos, T. L., Heme enzyme structure and function. *Chem. Rev.* **2014**, *114*, 3919-3962.

2. Meunier, B.; de Visser, S. P.; Shaik, S., Mechanism of oxidation reactions catalyzed by cytochrome P450 enzymes. *Chem. Rev.* **2004**, *104*, 3947-3980.

3. Banerjee, R.; Ragsdale, S. W., The many faces of vitamin B12: catalysis by cobalamin-dependent enzymes. *Annu. Rev. Biochem.* **2003**, *72*, 209-247.

4. Toraya, T., Radical catalysis in coenzyme B12-dependent isomerization (eliminating) reactions. *Chem. Rev.* **2003**, *103*, 2095-2127.

5. Gruber, K.; Puffer, B.; Krautler, B., Vitamin B12-derivatives-enzyme cofactors and ligands of proteins and nucleic acids. *Chem. Soc. Rev.* **2011**, *40*, 4346-4363.

6. Melkozernov, A. N.; Barber, J.; Blankenship, R. E., Light harvesting in photosystem I supercomplexes. *Biochem.* **2006**, *45*, 331-345.

7. Vassiliev, S.; Bruce, D., Toward understanding molecular mechanisms of light harvesting and charge separation in photosystem II. *Photosynth. Res.* **2008**, *97*, 75-89.

8. Scheller, S.; Goenrich, M.; Boecher, R.; Thauer, R. K.; Jaun, B., The key nickel enzyme of methanogenesis catalyses the anaerobic oxidation of methane. *Nature* **2010**, *465*, 606-608.

9. Kadish, K. M.; Smith, K. M.; Guilard, R., *The Porphyrin Handbook: Inorganic, organometallic and coordination chemistry*. Elsevier: 2000; Vol. 3.

10. Lindoy, L. F., Transition metal complexes of synthetic macrocyclic ligands. *Chem. Soc. Rev.* **1975**, *4*, 421-441.

11. Couch, P. W.; Games, D. E.; Jackson, A. H., Synthetic and biosynthetic studies of porphyrins. Part 1. Synthesis of the 'S-411' porphyrin obtained from meconium. *J. Chem. Soc., Perkin Trans. 1* **1976**, 2492-2501.

12. Rothemund, P., Formation of Porphyrins from Pyrrole and Aldehydes. *J. Am. Chem. Soc.* **1935**, *57*, 2010-2011.

13. Eschenmoser, A.; Wintner, C. E., Natural product synthesis and vitamin B12. *Science* **1977**, *196*, 1410-1420.

14. Sessler, J. L.; Tomat, E., Transition-metal complexes of expanded porphyrins. *Acc. Chem. Res.* **2006**, *40*, 371-379.

15. Fukuda, T.; Kobayashi, N., Hydrogenated Tetraazapophyrins. *Dalton Trans.* **2008**, *35*, 4673-4812.

16. Lee, C. H.; Dogutan, D. K.; Nocera, D. G., Hydrogen generation by hangman metalloporphyrins. *J. Am. Chem. Soc.* **2011**, *133*, 8775-8777.

17. Senge, M. O., Exercises in molecular gymnastics-bending, stretching and twisting porphyrins. *Chem. Commun.* **2006**, 243-256.

18. Satake, A.; Kobuke, Y., Dynamic supramolecular porphyrin systems. *Tetrahedron* **2005**, *61*, 13-41.

19. McGuire Jr, R.; Dogutan, D. K.; Teets, T. S.; Suntivich, J.; Shao-Horn, Y.; Nocera, D. G., Oxygen reduction reactivity of cobalt(II) hangman porphyrins. *Chem. Sci.* **2010**, *1*, 411.

20. Rosenthal, J.; Chng, L. L.; Fried, S. D.; Nocera, D. G., Stereochemical control of H_2O_2 dismutation by hangman porphyrins. *Chem. Commun.* **2007**, 2642-2644.

21. Bediako, D. K.; Solis, B. H.; Dogutan, D. K.; Roubelakis, M. M.; Maher, A. G.; Lee, C. H.; Chambers, M. B.; Hammes-Schiffer, S.; Nocera, D. G., Role of pendant proton relays and proton-coupled electron transfer on the hydrogen evolution reaction by nickel hangman porphyrins. *Proc. Natl. Acad. Sci. U.S.A.* **2014**, *111*, 15001-15006.

22. Losse, S.; Vos, J. G.; Rau, S., Catalytic hydrogen production at cobalt centres. *Coord. Chem. Rev.* **2010**, *254*, 2492-2504.

23. Mahammed, A.; Gross, Z., Corroles as triplet photosensitizers. *Coord. Chem. Rev.* **2017**.

24. Sorokin, A. S., Phtalocyanine metal complexes in catalysis. *Chem. Rev.* **2013**, *113*, 8152-8191.

25. Artero, V.; Chavarot-Kerlidou, M.; Fontecave, M., Splitting water with cobalt. *Angew. Chem. Int. Ed.* **2011**, *50*, 7238-7266.

26. Che, C. M.; Huang, J. S., Metalloporphyrin-based oxidation systems: from biomimetic reactions to application in organic synthesis. *Chem. Commun.* **2009**, 3996-4015.

27. Maeda, C.; Taniguchi, T.; Ogawa, K.; Ema, T., Bifunctional catalysts based on m-phenylene-bridged porphyrin dimer and trimer platforms: synthesis of cyclic carbonates from carbon dioxide and epoxides. *Angew. Chem. Int. Ed.* **2015**, *54*, 134-138.

28. Kalyanasundaram, K.; Graetzel, M., Artificial photosynthesis: biomimetic approaches to solar energy conversion and storage. *Curr. Opin. Biotechnol.* **2010**, *21*, 298-310.

29. Martinez-Diaz, M. V.; de la Torre, G.; Torres, T., Lighting porphyrins and phthalocyanines for molecular photovoltaics. *Chem. Commun.* **2010**, *46*, 7090-7108.

30. Teo, R. D.; Hwang, J. Y.; Termini, J.; Gross, Z.; Gray, H. B., Fighting Cancer with Corroles. *Chem. Rev.* **2017**, *117*, 2711-2729.

31. O'Connor, A. E.; Gallagher, W. M.; Byrne, A. T., Porphyrin and nonporphyrin photosensitizers in oncology: preclinical and clinical advances in photodynamic therapy. *Photochem. Photobiol.* **2009**, *85*, 1053-1074.

32. Mueller, E.; Bernardinelli, G.; Von Zelewsky, A., A new macrocyclic ligand combining two different coordination sites: macrocyclic biquinazoline (Mabiq-). Synthesis and structure of the free ligand and of a cobalt(III) complex. *Inorg. Chem.* **1988**, *27*, 4645-4651.

33. Banerjee, P.; Company, A.; Weyhermuller, T.; Bill, E.; Hess, C. R., Zn and Fe complexes containing a redox active macrocyclic biquinazoline ligand. *Inorg. Chem.* **2009**, *48*, 2944-2955.

34. Puttock, E. V.; Banerjee, P.; Kaspar, M.; Drennen, L.; Yufit, D. S.; Bill, E.; Sproules, S.; Hess, C. R., A Series of [Co(Mabiq)Cl_{2-n}] (n = 0, 1, 2) Compounds and Evidence for the Elusive Bimetallic Form. *Inorg. Chem.* **2015**, *54*, 5864-5873.

35. Kaspar, M.; Altmann, P. J.; Pothig, A.; Sproules, S.; Hess, C. R., A macrocyclic 'Co(0)' complex: the relevance of ligand non-innocence to reactivity. *Chem. Commun.* **2017**, *53*, 7282-7285.

36. Grübel, M.; Bosque, I.; Altmann, P. J.; Bach, T.; Hess, C. R., Redox and photocatalytic properties of a Ni^{II} complex with a macrocyclic biquinazoline (Mabiq) ligand. *Chem. Sci.* **2018**, *9*, 3313-3317.

37. Lazorski, M. S.; Castellano, F. N., Advances in the light conversion properties of Cu(I)-based photosensitizers. *Polyhedron* **2014**, *82*, 57-70.

38. Fischer, S.; Hollmann, D.; Tschierlei, S.; Karnahl, M.; Rockstroh, N.; Barsch, E.; Schwarzbach, P.; Luo, S.-P.; Junge, H.; Beller, M.; Lochbrunner, S.; Ludwig, R.; Brückner, A., Death and Rebirth: Photocatalytic Hydrogen Production by a Self-Organizing Copper-Iron System. *ACS Catalysis* **2014**, *4*, 1845-1849.

39. Cuttell, D. G.; Kuang, S. M.; Fanwick, P. E.; McMillin, D. R.; Walton, R. A., Simple Cu(I) complexes with unprecedented excited-state lifetimes. *J. Am. Chem. Soc.* **2002**, *124*, 6-7.

40. Mejia, E.; Luo, S. P.; Karnahl, M.; Friedrich, A.; Tschierlei, S.; Surkus, A. E.; Junge, H.; Gladiali, S.; Lochbrunner, S.; Beller, M., A noble-metal-free system for photocatalytic hydrogen production from water. *Chem. Eur. J.* **2013**, *19*, 15972-15978.

41. Cunningham, C. T.; Cunningham, K. L.; Michalec, J. F.; McMillin, D. R., Cooperative Substituent Effects on the Excited States of Copper Phenanthrolines. *Inorg. Chem.* **1999**, *38*, 4388-4392.

42. Paria, S.; Reiser, O., Copper in Photocatalysis. *Chem. Cat. Chem.* **2014**, *6*, 2477-2483.

43. Reiser, O., Shining Light on Copper: Unique Opportunities for Visible-Light-Catalyzed Atom Transfer Radical Addition Reactions and Related Processes. *Acc. Chem. Res.* **2016**, *49*, 1990-1996.

44. Zhang, Y.; Schulz, M.; Wächtler, M.; Karnahl, M.; Dietzek, B., Heteroleptic diimine–diphosphine Cu(I) complexes as an alternative towards noble-metal based photosensitizers: Design

strategies, photophysical properties and perspective applications. *Coord. Chem. Rev.* **2018**, *356*, 127-146.

45. Zeng, C.; Wang, N.; Peng, T.; Wang, S., Copper(I) Complexes Bearing 1,2-Phenyl-Bridged P^N, P^N^P, and N^P^N Chelate Ligands: Structures and Phosphorescence. *Inorg. Chem.* **2017**, *56*, 1616-1625.

46. In Mabiq complexes the Cu_c-$N_{diketim}$ bond length is typically shorter than the Cu_c-N_{bpm} bond length.

47. The coordinating deprotonoated Mabiq ligand carries a 1- charge, which is omitted for clarity and only considered in the overall charge of the complex. Ligand based radicals are denoted by a dot, the resulting negative charge is only considered in the overall charge of the complex.

48. Coppens, P.; Sokolow, J.; Trzop, E.; Makal, A.; Chen, Y., On the Biexponential Decay of the Photoluminescence of the Two Crystallographically-Independent Molecules in Crystals of [Cu(I)(phen)(PPh_3)$_2$][BF_4]. *J. Phys. Chem. Lett.* **2013**, *4*, 579-582.

49. Rader, R. A.; McMillin, D. R.; Buckner, M. T.; Matthews, T. G.; Casadonte, D. J.; Lengel, R. K.; Whittaker, S. B.; Darmon, L. M.; Lytle, F. E., Photostudies of 2,2'-bipyridine bis(triphenylphosphine)copper(1+), 1,10-phenanthroline bis(triphenylphosphine)copper(1+), and 2,9-dimethyl-1,10-phenanthroline bis(triphenylphosphine)copper(1+) in solution and in rigid, low-temperature glasses. Simultaneous multiple emissions from intraligand and charge-transfer states. *J. Am. Chem. Soc.* **1981**, *103*, 5906-5912.

50. Meghdadi, S.; Amirnasr, M.; Schenk, K. J.; Dehghanpour, S., Synthesis, Characterization, and Crystal Structures of $[Cu(ca_2en)_2]ClO_4$, and $[Cu(ca_2en)(PPh_3)_2]ClO_4$ Complexes. *Helv. Chim. Acta* **2002**, *85*, 2807-2816.

51. Oliver, S. W.; Smith, T. D.; Hanson, G. R.; Lahy, N.; Pilbrow, J. R.; Sinclair, G. R., Electron spin resonance study of the copper(II) and cobalt(II) chelates of 2,3; 7,8; 12,13; 17,18-tetrakis-(9,10-dihydroanthracene-9,10-diyl)porphyrazine. *J. Chem. Soc., Faraday Trans. 1* **1988**, *84*, 1475-1489.

52. Cunningham, K. L.; McNett, K. M.; Pierce, R. A.; Davis, K. A.; Harris, H. H.; Falck, D. M.; McMillin, D. R., EPR Spectra, Luminescence Data, and Radiationless Decay Processes of Copper(II) Porphyrins. *Inorg. Chem.* **1997**, *36*, 608-613.

53. The values given are the average and the corresponding standard deviation obtained from three independent measurements.

54. Uemura, T.; Furumoto, M.; Nakano, T.; Akai-Kasaya, M.; Saito, A.; Aono, M.; Kuwahara, Y., Local-plasmon-enhanced up-conversion fluorescence from copper phthalocyanine. *Chem. Phys. Lett.* **2007**, *448*, 232-236.

55. Nishikawa, M.; Nomoto, K.; Kume, S.; Inoue, K.; Sakai, M.; Fujii, M.; Nishihara, H., Dual Emission Caused by Ring Inversion Isomerization of a 4-Methyl-2-pyridyl-pyrimidine Copper(I) Complex. *J. Am. Chem. Soc.* **2010**, *132*, 9579-9581.

56. Healy, P. C.; Hanna, J. V., Tris(triphenylphosphine)copper(I) hexafluorophosphate. *Acta Crystallogr. Section E* **2003**, *59*, 384-386.

57. Hanson, G. R.; Gates, K. E.; Noble, C. J.; Griffin, M.; Mitchell, A.; Benson, S., XSophe-Sophe-XeprView. A computer simulation software suite (v. 1.1.3) for the analysis of continuous wave EPR spectra. *J. Inorg. Biochem.* **2004**, *98*, 903-916.

58. Apex. *APEX suite of crystallographic software, APEX 2, version 2008.4.*, Bruker AXS Inc., Madison, Wisconsin, USA (2008).

59. Wilson, A. J. C., International Tables for Crystallography. *International Tables for Crystallography*, Dordrecht, The Netherlands, Kluwer Academic Publishers (1992).

60. Hübschle, C. B.; Sheldrick, G. M.; Dittrich, B., SHELXLE. *SHELXLE, J. Appl. Crystallogr.* **2011**, *44*, 1281-1284.

61. Sheldrick, G. M., SHELXL-2014. *SHELXL-2014*, University of Göttingen, Göttingen, Germany (2014).

62. Sheldrick, G. M., SHELXL-97. *SHELXL-97*, University of Göttingen, Göttingen, Germany (1998).

63. Spek, A. L., *J. Appl. Cryst.* **2003**, *36*, 7-13.

64. Spek, A. L., *Acta Cryst.* **2009**, *D65*, 148-155.

65. Neese, F., The ORCA program system. *WIREs Comput. Mol. Sci.* **2012**, *2*, 73-78.

66. Neese, F., ORCA - an ab initio, DFT and semiempirical SCF-MO

package, version 3.0.2; Max Planck Insitut für Bioanorganische

Chemie: Mülheim an der Ruhr, Germany, 2009.

67. Becke, A. D., Density- functional thermochemistry. III. The role of exact exchange. *J. Chem. Phys* **1993**, *98*, 5648-5652.

68. Lee, C.; Yang, W.; Parr, R. G., Development of the Colle-Salvetti correlation-energy formula into a functional of the electron density. *Phys. Rev. B* **1988**, *37*, 785-789.

69. Becke, A. D., A new mixing of Hartree-Fock and local density-functional theories. *J. Chem. Phys.* **1993**, *98*, 1372-1377.

70. Becke, A. D., Density functional calculations of molecular bond energies. *J. Chem. Phys.* **1986**, *84*, 4524-4529.

71. Schäfer, A.; Horn, H.; Ahlrichs, R., Fully optimized contracted Gaussian basis sets for atoms Li to Kr. *J. Chem. Phys.* **1992**, *97*, 2571-2577.

72. Schäfer, A.; Huber, C.; Ahlrichs, R., Fully optimized contracted Gaussian basis sets of triple zeta valence quality for atoms Li to Kr. *J. Chem. Phys.* **1994**, *100*, 5829-5835.

73. Vahtras, O.; Almlöf, J.; Feyereisen, M. W., Integral approximations for LCAO-SCF calculations. *Chem. Phys. Lett.* **1993**, *213*, 514-518.

74. Baerends, E. J.; Ellis, D. E.; Ros, P., Self-consistent molecular Hartree-Fock-Slater calculations I. The computational procedure. *J. Chem. Phys.* **1973**, *2*, 41-51.

75. Dunlap, B. I.; Connolly, J. W. D.; Sabin, J. R., On some approximations in applications of Xα theory. *J. Chem. Phys.* **1979**, *71*, 3396-3402.

76. Eichkorn, K.; Treutler, O.; Öhm, H.; Häser, M.; Ahlrichs, R., Auxiliary basis sets to approximate Coulomb potentials. *Chem. Phys. Lett.* **1995**, *240*, 283-290.

77. Eichkorn, K.; Weigend, F.; Treutler, O.; Ahlrichs, R., Auxiliary basis sets for main row atoms and transition metals and their use to approximate Coulomb potentials. *Theor. Chem. Acc.* **1997**, *97*, 119-124.

78. Noodleman, L., Valence bond description of antiferromagnetic coupling in transition metal dimers. *J. Chem. Phys.* **1981**, *74*, 5737-5743.

79. Noodleman, L.; Davidson, E. R., Ligand spin polarization and antiferromagnetic coupling in transition metal dimers. *J. Chem. Phys.* **1986**, *109*, 131-143.

80. A. T. Amos, G. G. H., Single determinant wave functions. *Proc. R. Soc. London. Ser. A.* **1961**, *263*, 483-493.

81. King, H. F.; Stanton, R. E.; Kim, H.; Wyatt, R. E.; Parr, R. G., Corresponding Orbitals and the Nonorthogonality Problem in Molecular Quantum Mechanics. *J. Chem. Phys.* **1967**, *47*, 1936-1941.

82. Neese, F.; Olbrich, G., Efficient use of the resolution of the identity approximation in time-dependent density functional calculations with hybrid density functionals. *Chem. Phys. Lett.* **2002**, *362*, 170-178.

83. Humphrey, W.; Dalke, A.; Schulten, K., VMD: visual molecular dynamics. *J. Mol. Graph.* **1996**, *14*, 33-38, 27-38.

For Table of Contents Only.

A series of mono- and bimetallic copper-Mabiq complexes is described. One-electron reduction of the Cu^{II} and $Cu^{I}Cu^{II}$ complexes is ligand-centered, yielding the (Mabiq$^{\bullet}$) form of the macrocycle. Both bimetallic compounds are thus mixed-valent with respect to the metal ions. The influence of the outer copper ion on the redox, spectroscopic and photochemical properties of the central ion was examined. The two metals ions interact weakly, such that the photoactivity of the central Cu-Mabiq unit is retained.